JOURNAL OF GEOPHYSICAL RESEARCH, VOL. 98, NO. B8, PAGES 14,321–14,337, AUGUST 10, 1993

# Impact and Volcanism: A Momentum Scaling Law for Erosion

CHARLES H. SIMONDS

*Lockheed Missiles & Space Company Incorporated, Houston, Texas*

SUSAN WERNER KIEFFER

*Department of Geology, Arizona State University, Tempe*

The controversy that raged through the 1950s–1970s over similarities and differences between meteorite impact and volcanic processes is revisited in this paper. We propose that there are quantitative similarities in erosion caused by high-speed ejecta produced by either impacts or volcanic processes. Field and petrographic data from the Manicouagan impact crater, Canada, are used to demonstrate that during the emplacement of the impact melt sheet, erosion occurred at a rate of ~2562 kg $m^{-2}$ $s^{-1}$. Field data for the Mount St. Helens lateral blast of May 18, 1980, suggest an erosion rate of 21 kg $m^{-2}$ $s^{-1}$, and field data for a small pyroclastic flow on August 7, 1980, suggest an erosion rate of ~14 kg $m^{-2}$ $s^{-1}$. It is proposed that these three rates were determined dominantly by the momentum of the ejecta, and a quantitative formulation based on lofting theory is given. A new application of the Monte Carlo approach to analysis provides minimum, most likely, and maximum estimates for both the field and the theoretical analyses. The substantial erosion that occurs by fast moving flows results in mixing of stratigraphic components over large distances and to very fine scales.

## 1. INTRODUCTION

The controversy over the origin of lunar craters sparked much debate regarding the nature of volcanic and meteorite impact processes from the 1950s–1970s [*Dence*, 1965]. Detailed fieldwork pioneered by *Shoemaker*'s [1963] classic work on Meteor Crater, Arizona; petrographic studies of the results of shock wave processes on rocks [*French and Short*, 1968]; laboratory studies on the equations of state of shocked rocks [*Ahrens and O'Keefe*, 1977]; and large computer models (*Ahrens and O'Keefe* [1987] and earlier works) contributed to major advances in the understanding of impact processes and the origin of impact craters on the Moon and other planets. Quantitative understanding of volcanic processes developed somewhat later. The understanding was sparked by new documentation of volcanic processes in Hawaii, Japan, and, particularly, at Mount St. Helens in 1980 (see *Lipman and Mullineaux* [1981] for an example of this synthesis). The opportunity to correlate the characteristics of field deposits to dynamics observed during eruptions has contributed to an expansion in our understanding of volcanic processes. These developments from the 1970s to now are comparable to the advances made in understanding planetary impact craters during the peak years of manned and unmanned planetary exploration. Application of fluid dynamics concepts to volcanic processes was pioneered by L. Wilson and coworkers (see, for example, the review by *Wilson et al.* [1987]). Large computer models now provide insight into dynamic processes. For example, *Kieffer* [1984] used a Rocketdyne nozzle model to improve calculational accuracy for her proposed model for supersonic flow during the lateral blast at Mount St. Helens [*Kieffer*, 1981]. Supercomputer models can now be used to examine the influence of a number of geometric and fluid-dynamical parameters on volcanic eruption processes [*Wohletz et al.*, 1984; *Valentine and Wohletz*, 1989, 1991; *Valentine et al.*, 1992]. However, no recent work has revisited the interesting possibility of comparing and contrasting impact and volcanic processes.

In this paper we make such a revisitation by examining erosion of surfaces affected by volcanic flows and impact ejecta. We summarize observations of erosion at the Manicouagan, Quebec, impact structure and at two flows at Mount St. Helens: the lateral blast of May 18, 1980, and the channeled pyroclastic flow of August 7, 1980. We constrain estimates of the erosion rate by estimating volume and surface area eroded as well as event duration. We estimate the velocity, viscosity, and density of the eroding fluids in each case. We use a simple theory for the rate of erosion that requires estimated velocities, viscosities, and densities, and we compare the calculated rates of erosion with those estimated from field data.

## 2. IMPACT-INDUCED EROSION AND MIXING

### 2.1. *Geologic Observations of Erosion and Mixing at Manicouagan*

One of the most intensely studied craters that contains impact-mixed lithologies is the 65-km Manicouagan structure in eastern Quebec (Figure 1). Papers summarizing the data about the crater were presented as a group in the *Journal of Geophysical Research* (*83*, 2729–2815, 1978). The Manicouagan impact structure is dated at latest Triassic: 214 ± 5 m.y. ago by a Rb–Sr mineral isochron [*Jahn et al.*, 1978] and 210 ± 8 m.y. ago by potassium-argon techniques [*Wolfe*, 1971]. *Olsen and Sues* [1984] suggested that the Manicouagan impact may have been responsible for an extinction in the terrestrial vertebrate population. The possibility would be enhanced if the true age is at the younger extreme of the analytical error bars of the age determinations.

The bedrock at Manicouagan consists of a variety of intermediate to granitic gneisses enclosing a deformed, layered igneous complex ranging in composition from gabbro to anorthosite. These basement lithologies were metamor-

Copyright 1993 by the American Geophysical Union.

Paper number 93JB00704.
0148-0227/93/93JB-00704$05.00

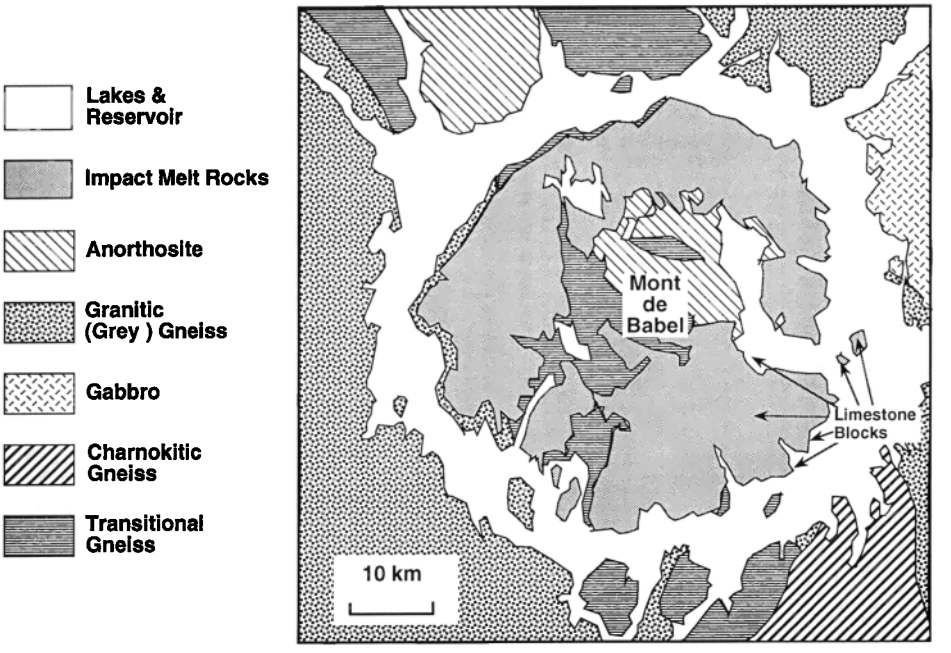


Fig. 1. Geologic map of the Manicouagan structure. The melt sheet covers most of the island around the remnant of the central peak, Mont de Babel. The inner edge of the ring-shaped reservoir marks the periphery of the preserved melt sheet. The circular reservoir appears to occupy the places of intense glacial erosion of the fractured rock along the periphery of impact crater. The Manic Cinq Dam is located just south of the area shown.

phosed to amphibolite facies and deformed one or more times, culminating in the Grenville event 932 ± 14 m.y. ago [*Wolfe*, 1971]. At the time of impact the basement was overlain by a veneer of Ordovician limestone (see below). Different field-mappable lithologies are separated from each other by several kilometers, a fact to which we will return in the discussion of mixing (section 2.2.).

In its current state of preservation the structure of Manicouagan is dominated by a large melt sheet that overlies and includes blocks of allocthonous limestone and a moderately shocked central structure. The 100-m-thick impact melt sheet forms an annular ring extending 7–29 km from the center. Glacial erosion completely removed the portion of the melt sheet farthest from the center. We estimate that the sheet extended at least a kilometer beyond the farthest preserved section. Thus the preerosion melt sheet was a minimum of 30 km in diameter.

The center of Manicouagan is marked by a well-defined central peak, Mont de Babel. The upper part of the central peak consists of anorthosite partially transformed to maskelynite (shock-vitrified feldspar). Allocthonous blocks of Ordovician limestone occur near the base of the melt sheet inside the reservoir (Figure 1). The relative structural position of these blocks is 500 m below the unbrecciated basement outside the reservoir. This relation indicates that the basement inside the reservoir has been displaced downward a minimum of 500 m relative to the basement outside the reservoir. The allocthonous limestone blocks range up to 10 m in diameter. They do not exist in their inferred original stratigraphic position (veneer over unshocked bedrock) but have been scraped up and incorporated into the melt sheet. The 10-m minimum diameter of observed blocks establishes a minimum limit of erosion of 10 m in the areas of limestone occurrence.

The original topographic rim of the crater at Manicouagan appears to be near the outer edge of the reservoir that is currently backed up behind Quebec Hydro's Manic Cinq (Daniel Johnson) Dam (Figure 1). The diameter of the transient cavity (as contrasted to the final crater) is not well constrained. The innermost occurrences of Ordovician limestone and the geophysical modeling of *Sweeny* [1978] suggest a range of 30–44 km. *Grieve and Head* [1983] suggest a transient cavity of 60 km (Table 1) based on a different interpretation of the stratigraphic position of limestone blocks and interpretation of shock deformation features in the basement [*Dressler*, 1970]. We use 44 km as a representative estimate for scaling purposes and cite some results for the extremes of 30 and 60 km. Uplifted maskelynite-bearing rocks in the center of the structure and downwardly displaced limestone blocks around these suggest that the crater had a central uplift peak or peak ring.

The base of the melt sheet is typically a sharp (<1 cm) contact between melt rock and underlying quartzofeldspathic gneisses. There is no evidence of preserved limestone veneer, karst topography, weathered soils, or the inverted stratigraphy of host rock typically seen at smaller craters (e.g., Meteor Crater, Arizona [*Shoemaker*, 1963]). However, in a few local places, pockets of moderately lithified breccias containing more than 50% recognizable clasts, with no maskelynite and few shock deformation features, separate the melt sheet from the underlying basement. These pockets may represent the unmelted shocked material that was emplaced before the melt sheet (see section 2.3 and Figures 3–8). The pockets are a few meters thick and extend laterally no more than 200 m. The base of the melt sheet has local relief of up to 10 m. The local relief occurs as both smooth undulations in the surface and sharp faultlike offsets around which melt flowed. This relation indicates that the sharp offsets predate solidification of the melt.

TABLE 1. Projectile Diameter and Energy Scaled From Relations of *Schmidt and Housen* [1987]

| | Ice[a] | Permafrost[b] | Diabase[c] | Diabase[d] |
|---|---|---|---|---|
| Density, kg $m^{-3}$ | 910 | 1960 | 3000 | 3000 |
| Velocity, m $s^{-1}$ | 57,700 | 57,700 | 24,600 | 17,000 |
| | *Spherical Projectile Diameter, m [Schmidt and Holsapple, 1982]* | | | |
| Transient cavity diameter, m | | | | |
| 60,000[e] | 5,250 | 3,810 | 5,125 | 6,300 |
| 44,000[f] | 3,530 | 2,560 | 3,450[g] | 4,230 |
| 30,000[h] | 2,180 | 1,580 | 2,130 | 2,610 |
| | *Kinetic Energy, J* | | | |
| 60,000[e] | 1.15E+23 | 9.45E+22 | 6.40E+22 | 5.68E+22 |
| 44,000[f] | 3.49E+22 | 2.87E+22 | 1.95E+22[g] | 1.72E+22 |
| 30,000[h] | 8.22E+21 | 6.74E+21 | 4.59E+21 | 4.04E+21 |

Read 1.15E+23 as $1.15 \times 10^{23}$.
[a]Projectile analogous to [*Shoemaker et al.*, 1990] comet case.
[b]Projectile analogous to [*Shoemaker et al.*, 1990] comet nucleus case.
[c]Projectile analogous to [*Shoemaker*, 1977] Earth-crossing asteroid.
[d]Projectile analogous to an asteroid with impact at velocity equal to micrometeorites [*Zook*, 1975].
[e]Transient cavity estimated by *Grieve and Head* [1983] emphasizing localized high shock pressure estimates in basement.
[f]Upper bound of transient cavity estimate of *Phinney et al.* [1978]; and *Floran et al.* [1978], limited by occurrence of limestone blocks.
[g]Indicates preferred estimate used to scale Figures 3–8.
[h]Lower bound of transient cavity estimate of *Phinney et al.*, [1978]; and *Floran et al.* [1978].

The melt sheet has two vertically stacked units that are texturally different, referred to here as the lower and upper units. The top of the upper unit is not preserved. The grain size of the groundmass crystals (plagioclase, potassium, feldspar, quartz, and augite) in the upper unit increases upward, which, we assume by comparison with textures in igneous melt sheets, indicates that the center of the melt sheet lay above any observed outcrop. The thickest stratigraphic section through the melt measured 108 m. Measured thicknesses nearly as great occur in several different parts of the melt sheet, suggesting that the thickest measured section was not atypical. We infer that the coarse material now exposed at the top of the melt sheet was originally near the center and that roughly half the melt sheet has been eroded. In estimating the total volume of the melt sheet we have assumed that this eroded material added from 32–132 m to the 108-m maximum thickness measured, giving a total original thickness in the range of 150–250 m.

The melt sheet has a fine-grained matrix with microcrystals of plagioclase, clinopyroxene, potassium feldspar, and quartz. This melt sheet, like virtually all impact breccias, contains mixtures of materials of a wide range in shock states. Because of the monotonic decrease of shock pressure with distance from the center of the impact, the combination of lithologies in the melt sheet indicates intense mixing during emplacement. We define here the use of the term "impact melt" for the melt sheet because this sheet is the final product of mixing of the "shock melt" (the material that became molten during the rarefaction immediately following the shock compression phase) and other lightly to moderately shocked fragments that were subsequently mixed into the shock melt. As discussed below, the lesser to moderately shocked material was partially melted and mixed into the original shock melt. Thus the impact melt is compositionally (geochemically) and petrographically different from a pure shock melt. *Simonds et al.* [1978] demonstrated that the large crystals of quartz are clasts, not phenocrysts. Plagioclase is the liquidus phase of the melt. At the scale of petrographic thin sections the dominant foreign clasts are quartz crystals. In the finest-grained melt rocks some of these relict quartz grains are surrounded by reaction rims of intergrown quartz, alkali feldspar, and augite. These clasts are assumed to have been eroded from the country rock and entrained into the melt. These clasts average up to 9% of the lower unit of the melt sheet. Significantly, the remnant quartz crystals are largely free of planar structures or other features suggestive of exposure to shock pressures over 25 GPa. Thus the impact melt rock has few visible remnants of material shocked to pressures between 25 GPa and the melt limit of ~75 GPa.

The lower unit ranges in thickness from 45 to ~60 m and is in contact with the basement rock. It is an aphanitic impact melt with 1–9% clasts that are 84–100% quartz. Only a small fraction of these display any glass, devitrified textures, or planar structures that would suggest exposure to shock pressures in excess of 25 GPa, and so for simplicity we assume that the quartz crystals indicate incorporation of only unshocked to weakly shocked material.

The upper unit has no remnant crystals, and we assume that it contains little unshocked material but may contain some (undetectable) digested moderately shocked material. Additional debris was incorporated into the melt, including boulder-sized clasts that are up to 10 m in diameter. From (limited) exposures we infer that large blocks comprise <1% of the melt sheet. We ignore this component in further discussion.

### 2.2. *Geochemical Observations*

The geochemical observations of the Manicouagan melt sheet support the above suggestion that moderately shocked material was incorporated into the shock melt. These observations also suggest intense mixing of the target lithologies at a microscale (Figure 2). Analysis of $1.5 \times 10^{-3}$ kg aliquots

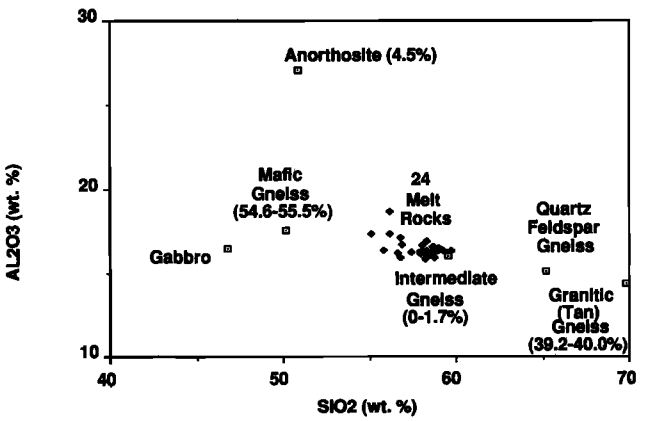


Fig. 2. $Al_2O_3$ versus $SiO_2$ for Manicouagan. The boxed dots mark the centers of compositional components identified for the target by *Grieve and Floran* [1978], and the percentages in parentheses reflect their estimate of the fraction of the melt sheet that can be attributed to each of those components. Each of the major compositional groups identified by *Grieve and Floran* [1978] generally correlates to the mappable units (Figure 1).

by X ray fluorescence shows a homogenization of the melt that can be explained by mixing of the dominant lithologies (components) present in the bedrock in different proportions (see compositional analyses and caption to Figure 2). During impact the flow process somehow blended at a microscale of millimeters to centimeters materials from different field-mappable lithologic units separated from one another by several kilometers. We do not consider here the still important problem of the fluid dynamics of the vapor-liquid-solid mixing problem. *Palme* [1982] conducted a search for meteoritic trace elements in the melt sheet and observed none of significance. Despite the evidence for intense mixing of the target the projectile does not appear to have left a geochemical signature in the melt.

### 2.3. *Flow During Impact Cratering at Manicouagan*

We present our view of the impact process at Manicouagan in Figures 3–8 with supporting data in Tables 1, 2, 3*a*, and 3*b*. The illustrations are based on the model of *Kieffer and Simonds* [1980] for a crater with a transient cavity diameter of 44 km. In order to make the estimates of volumes of melted, shocked, and unshocked ejecta required for this paper the energy of the meteorite must be inferred from the transient cavity dimensions, and then scaling of melt and ejecta volumes must be done from the energy estimate.

We do not know the type of projectile that formed Manicouagan or the impact velocity or angle of incidence. There is no evidence of meteoritic contamination at Manicouagan, so we exclude the possibility of impact of an iron meteorite, but a number of possibilities remain. *Shoemaker et al.* [1990] have suggested that most large terrestrial craters formed by impact of comets or comet nuclei, for which the impact velocity could be as high as 60 km $s^{-1}$. If the projectile were meteoritic in composition and originated in the asteroid belt, velocities in the range of 17–24 km $s^{-1}$ are more appropriate [*Shoemaker*, 1977; *Zook*, 1975].

To assess the impact of the uncertainties in impact conditions, we applied the scaling relations of *Schmidt and Housen* [1987] and *Melosh* [1989] to obtain a range of meteorite diameters that would produce transient cavities in the range of 30–60 km (Table 2). We use the intermediate value of 44 km for the preferred diameter of the transient cavity in subsequent calculations. Earlier estimates of energy from *Dence et al.* [1977] and *Phinney et al.* [1978] were made from scaling of energy of nuclear and experimental craters but give energies similar to the more recent estimates of *Schmidt and Housen* [1987] and *Holsapple and Schmidt* [1987] and are therefore used here. The energy estimate shown in Table 1 was used to constrain the quantities shown in Figures 3–8, which were derived using the equations of *Kieffer and Simonds* [1980].

We assume that the transient cavity was 44 km in diameter and that it was formed by a diabase meteorite impacting at 24.6 km $s^{-1}$. The Schmidt-Hosapple model gives a diameter of 3450 m for the meteorite and a kinetic energy of $1.95 \times 10^{22}$ J (Table 1). In Table 1, note that this diameter is intermediate between two others predicted by different models and is in the range that would be predicted for lower-density, higher-velocity ice or permafrost projectiles. We therefore feel that the model presented here is relatively independent of assumptions regarding the nature of the projectile and impact conditions.

The results that follow are quantitatively altered by choice of a different meteorite or impact velocity but are not qualitatively altered. For example, in Figures 3–8 we show isobars of peak shock pressure for the preferred values and models described above. The melt volume calculations of *O'Keefe and Ahrens* [1982] (Table 2) suggest that these isobars shift outward about 11% for a cometlike projectile impacting at 57.7 km $s^{-1}$ or 22% for a projectile that has the properties of a comet nucleus impacting at this higher velocity.

These figures are intended to illustrate our best understanding of many complicated phenomena, such as peak pressure isobars as a function of distance, time histories of shock movements, depth of penetration of the meteorite, and stratigraphic relations. We wish to emphasize for this discussion the movement out of the crater of material shocked to less than 25 GPa (weakly shocked) and the partial incorporation of unshocked material into the flowing shock melt. We propose that the shock melt continuously overtakes and digests or partially digests material of progressively lower shock degree. That is, material shocked to about 75 GPa is first overtaken and incorporated by the shock melt. This mixture then progressively overtakes material shocked to lower pressures. Material eroded and entrained early in the process is mechanically broken up and thermally digested for a longer time than material entrained later in the process. This scenario of the ejection and emplacement process is the basis for the erosion model below. To develop this scenario further, we need to estimate the volume of material shocked to pressures between 75 and 25 GPa and the volume shocked to pressures <25 GPa. This estimate is made by analysis of the final melt volume and petrographic characteristics. The erosion duration listed in Table 3*b* is the radius to the edge of the melt sheet divided by the fluid velocity.

We point out that the mixing and erosion processes that we are inferring from field and petrographic evidence are very complex and are beyond the current state of the art of computer modeling because of several problems: (1) the

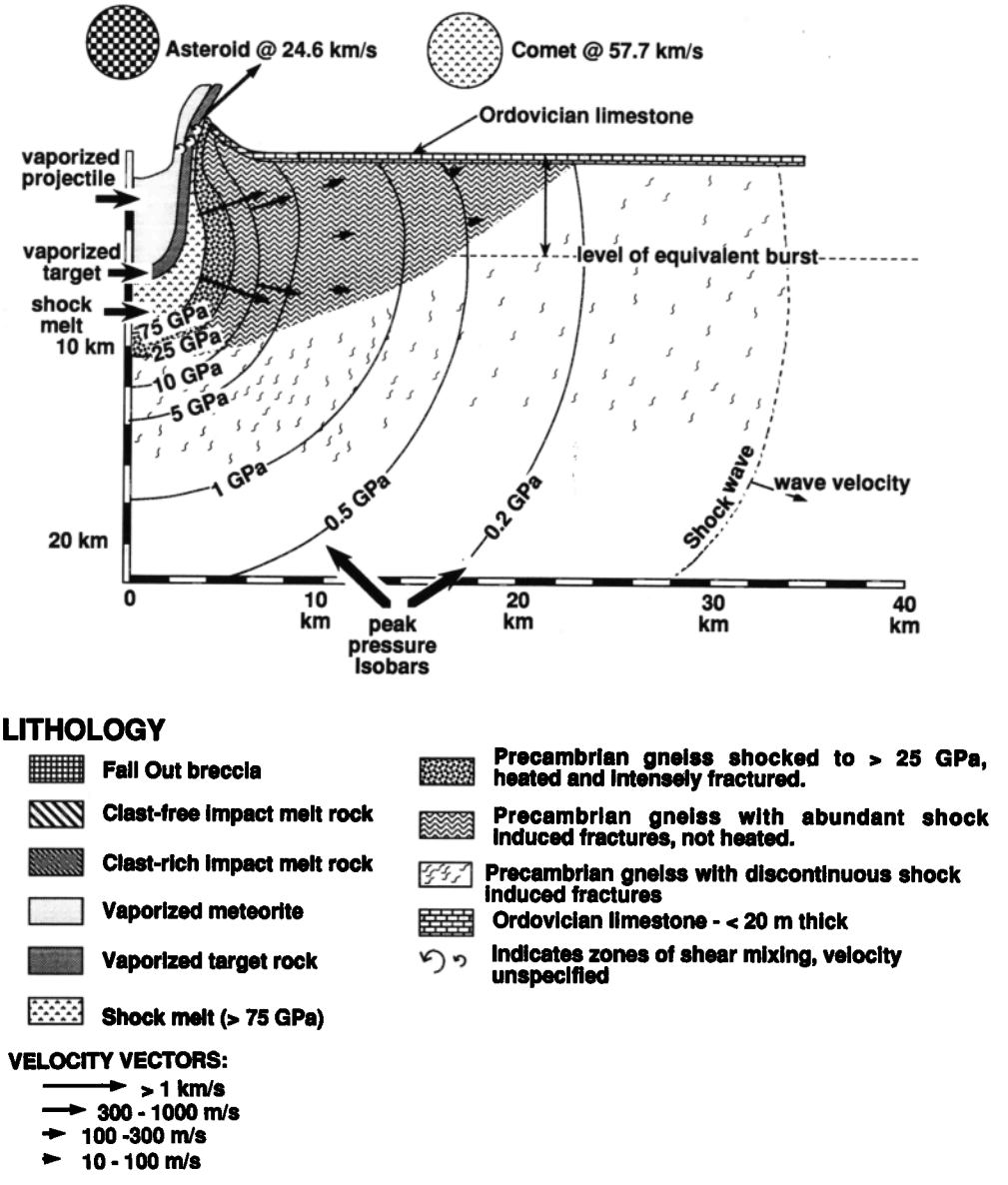


Fig. 3. Excavation ~3 s after contact. The time for this stage of the cratering event is estimated as the amount of time required for the projectile to penetrate to the indicated depth (based on the calculations of *O'Keefe and Ahrens* [1975], with scaling to the 4.4-km-diameter meteorite). The dashed horizontal line, here and in the subsequent drawings, marks the depth of an equivalent explosive burst at 5.4 km. In this, and subsequent drawings, the isobars represent peak shock pressures; the velocity vectors represent particle motion and represent the motion accumulated through the peak shock pressures and subsequent rarefactions. In subsequent figures the reader should compare and contrast: (1) the shock melt, (2) the material shocked to 25–75 GPa (the rocks that would contain shock-vitrified quartz and feldspar), and (3) the intensely fractured materials within the eventual boundary of the transient cavity. The shock melt has an average temperature of over 3000°C and a viscosity of $<10^{-2}$ Pa s, and the rocks in the zone between 25 and 75 GPa have a temperature of 200°–1300°C derived from data of *McQueen et al.* [1967]. Note that in this early phase of the excavation process the flow is orthogonal to the peak shock pressure isobars, which are treated as markers expanding much like an inflating balloon.

scale of mixing ranges from kilometers to millimeters, which is difficult to model computationally; (2) turbulent mixing laws are not well known nor is the rheology of the material involved in such a process; and (3) multicomponent, multiphase computations are still very difficult. We hope this paper points out the need for future research in these directions.

### 2.4. *Estimate of Impact Melt Volume, Eroded Volume, and Original Shock Melt Volume*

None of the values required to estimate the preerosion volume of the melt sheet, the volume of eroded debris, or the volume of the original shock melt are known precisely. Because these variables are to be combined algebraically to get other characteristic parameters, it is desirable to have not only an estimate of the median value for these volumes but also some estimate of the variance. Therefore the volumes were calculated probabilistically by Monte Carlo techniques. Minimum, most likely, and maximum values for each significant geometric or petrographic parameter, or for parameters required for the theory proposed later, are estimated (Table 3*a*) (from reports of *Simonds et al.* [1978] and *Floran et al.* [1978]).

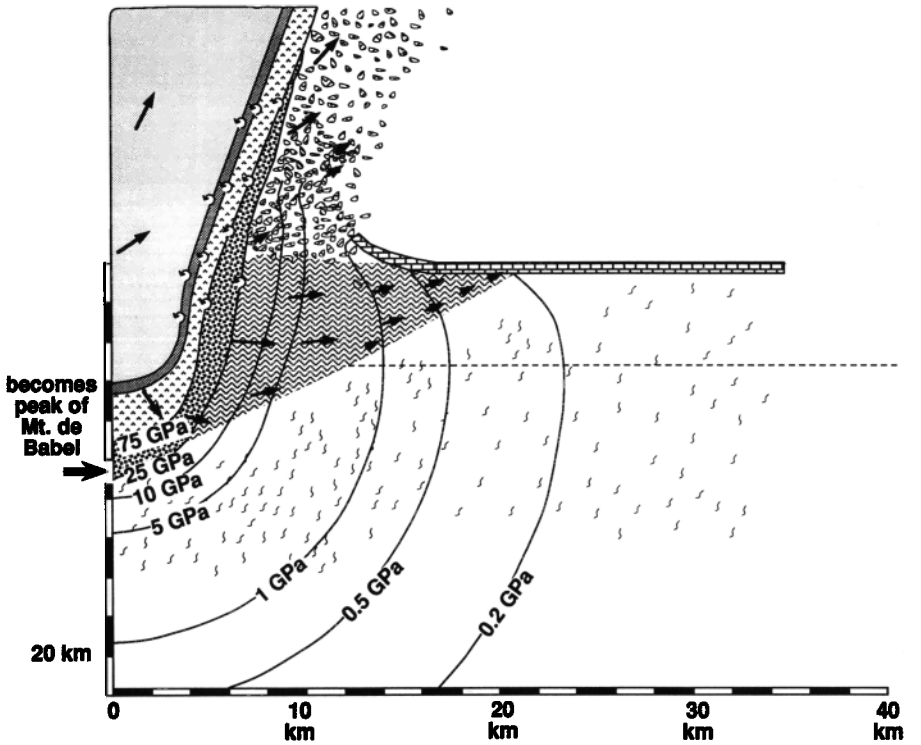


Fig. 4. Ejection ~20 s after contact. The time for this stage is estimated from the relations of *Melosh* [1989], who proposes that the amount of time required for the crater to grow to maximum depth is approximately equal to the time for an object initially at rest to fall that distance (~33 s). We have reduced this estimate to 20 s for this figure, because we are showing a configuration in which the crater has not yet reached maximum depth. By this time, thermal and kinetic energy and momentum are starting to be transferred from the hot-fast materials to the cold-slow ones by shearing and mixing. We speculate on the beginning and evolution of the mixing processes as follows: The superheated shock melt is initially confined to a region defined by roughly the 75-GPa isobar. When the rarefactions that follow the shock waves into the rock begin to rotate the velocity vectors from their original orientation normal to the peak pressure isobars to orientations subparallel to the peak pressure isobars, mixing occurs because of shear induced by velocity gradients. In contrast to the motion described in Figure 3 as a radial "balloonlike" expansion we envision the flow to be evolving to a configuration characterized by much more shear between fast moving central material and more slowly moving distal material. For example, the shock melt is starting to mix with the maskelynite-bearing rock at the time shown in this figure. Because the rarefactions originate at the projectile-ground interface, mixing initially occurs near the surface, as shown schematically by the mixing symbols (see Figure 3). In shocked volumes where compressional strains and velocity vectors are still dominantly normal to the peak shock pressure isobars, there is not yet much mixing (e.g., deeper in the crater). Numerical calculations of the flow field set up by impacts [*O'Keefe and Ahrens*, 1975, 1976; *Orphal*, 1977*a*, *b*] suggest that the maximum flow velocities have fallen off to several hundred meters per second and much material is moving half an order of magnitude slower. The Reynolds number of the silicate melt is well over $10^5$, implying turbulent flow, with density and viscosity listed in Table 3*a*, and flow velocity at several hundred meters per second. We envision a relatively thin zone, which we will call the "boundary layer," across which the flow velocity decreases dramatically from the order of hundreds of meters per second to nearly zero in the fragmented solids. This zone may correspond to the clast-rich lower zone of the melt sheet discussed in section 2.4. In the model calculations of section 4, which require an estimate of boundary layer thickness, we use values derived from this inference.

To obtain the volume of impact melt, we approximate the melt sheet as a flat cylindrical "washer" (see, for example, cross sections of *Floran et al.* [1978] for justification of this approximation). The volume $V$ of such a washer of thickness $T$, with an outer radius $R_{\text{outer}}$ containing a cylindrical hole with radius $R_{\text{inner}}$ is

$$V = \pi T(R_{\text{outer}}^2 - R_{\text{inner}}^2) \quad (1)$$

This would be the total volume of the impact melt sheet. We take the inner radius to vary between 7.5 and 11 km and the outer radius to be in the range of 22–30 km. The thickness $T$ is taken as 150–250 m, as discussed in section 2.1.

To estimate the amount of debris incorporated into the melt sheet, one must consider two separate problems: (1) the volume of unshocked material (i.e., included bedrock) that is partially represented by the remnant unshocked quartz clasts ($V_1$); and (2) the volume of moderately shocked debris (i.e., the volume of the material shocked to between 25 and 75 GPa and totally digested for which there is no visible remnant $V_2$).

$V_1$ and $V_2$ are obtained by considering the nature of the melt sheet in detail. To estimate $V_1$, we note that we pointed out in section 2.1 that all remnants of the weaker shocked material are in the lower unit. In order to estimate the total digested material from the measured abundance of quartz crystals the volume of quartz in the lower unit must first be estimated. Because nearly all other components of the target (such as feldspars, amphiboles, and biotite) have been totally melted after being mixed into the impact melt, one must infer their volume from knowledge of the quartz mode in the

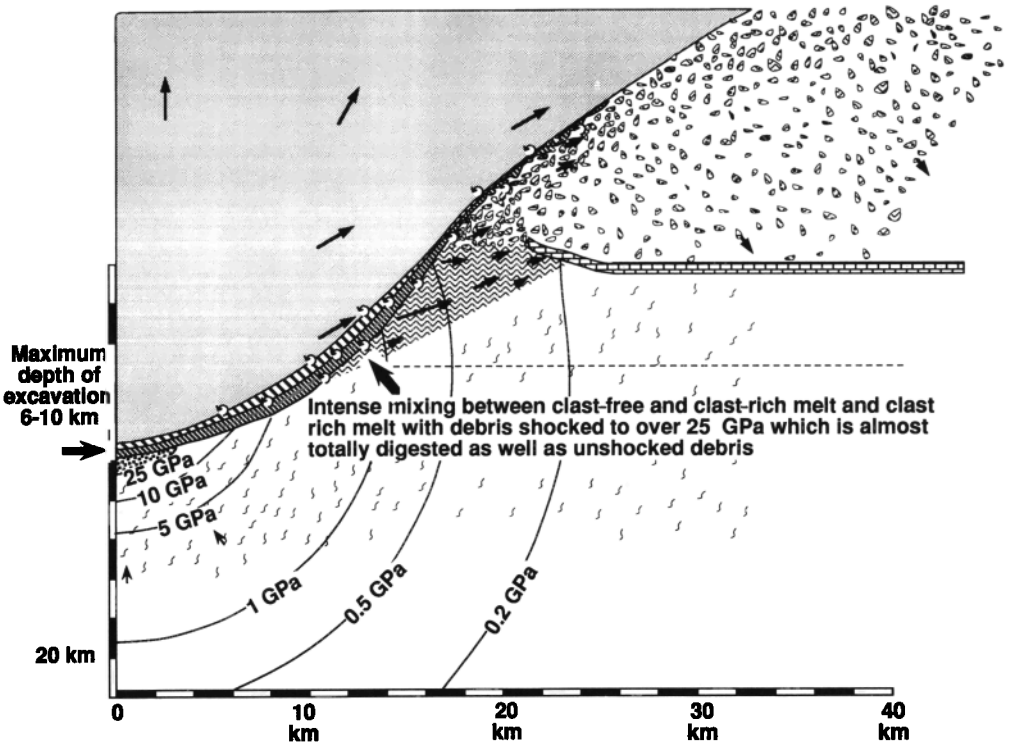


Fig. 5. External flow ~50 s. To estimate the time appropriate to this figure, we have taken *Melosh*'s [1989] estimate of 33 s for the crater to grow to maximum depth and have added about 20 s to account for the fact that this diagram shows a stage beyond that at which final depth is reached; the crater has begun to expand outward. Mixing and erosion continue, as shown by the symbols. The shock melt has become totally mixed with the maskelynite-bearing material, and the material shocked to over 25 GPa is probably already digested (i.e., mechanically incorporated and thermally breaking down). The mixture of shock melt and debris, now appropriately called "impact melt," has cooled down to the liquidus temperature, ~1200°C, and its viscosity has increased to ~120 Pa s. The melt sheet has expanded downward and outward until it has reached the lower boundary of the zone with abundant shock-induced features. Locally, pockets of moderately lithified breccia (discussed in section 1) are preserved as shown schematically.

target rock. To obtain $V_1$, we first determine the volume of the lower unit by multiplying the total melt sheet volume $V$ by the fraction $T_{cl}/T$, the ratio of the thickness of the lower unit to the total melt sheet (Figure 9 summarizes the nomenclature used here). $V_1$ consists of three components, preserved quartz clasts, preserved nonquartz clasts, and digested clasts. We estimate $V_1$ by determining the fraction of the volume of the lower unit that is quartz and then inferring that amount of basement rock that would have been mixed in to yield that much quartz. The volume of quartz in the lower unit is the product of the volume of the lower unit times the clast mode of the lower unit ($M_c$) times the fraction of the clasts that are quartz ($M_{qc}$). The total volume of debris corresponding to those quartz clasts is calculated by dividing the volume of quartz clasts by the quartz mode in the basement:

$$V_1 = V(T_{cl}/T)(M_c \times M_{qc})/M_q \qquad (2a)$$

The volume of stripped material shocked between 25 and 75 GPa ($V_2$) is very uncertain, and we simply estimated it from the relative volumes implied in Figures 3–8, allowing it to range from 0 to 50% of the total melt sheet with the best estimate taken as 20%. Finally, the volume of shock melt ($V_{sh}$) is given by

$$V_{sh} = V - V_1 - V_2 \qquad (2b)$$

Before presenting the results of the Monte Carlo calculations for $V$, $V_1$, $V_2$, and $V_{sh}$, we illustrate the above method by presenting the geometric model and by using a single set of numbers based on the best estimates for the input parameters. After this development and illustration we give the results from the Monte Carlo calculations of the same quantities. The variables calculated from the best estimates of the individual input parameters typically differ from the median values given by the Monte Carlo simulator because of the asymmetry of the distribution of input parameters. The Monte Carlo medians are typically, but not always, larger than the estimates arrived at using the best estimates of input parameters. This pattern results from the fact that the difference between the minimum and most likely values is typically smaller than the difference between the most likely and maximum values. The individual estimates of $V$, $V_1$, and $V_2$ that are made by the Monte Carlo simulator can result in a relatively large $V$ being associated with a small $V_1$ or $V_2$ and vice versa. Thus the minimum (16th percentile), median (50th percentile), and maximum (84th percentile) sizes of each result should not be expected to add up to 100%. As an example, if one takes the individual numbers associated with the 16th percentile, $V_{sh}^{16} \neq V^{16} - V_1^{16} - V_2^{16}$, where the superscript denotes the value specific to the Monte Carlo model.

For the most likely values of the parameters listed in Table

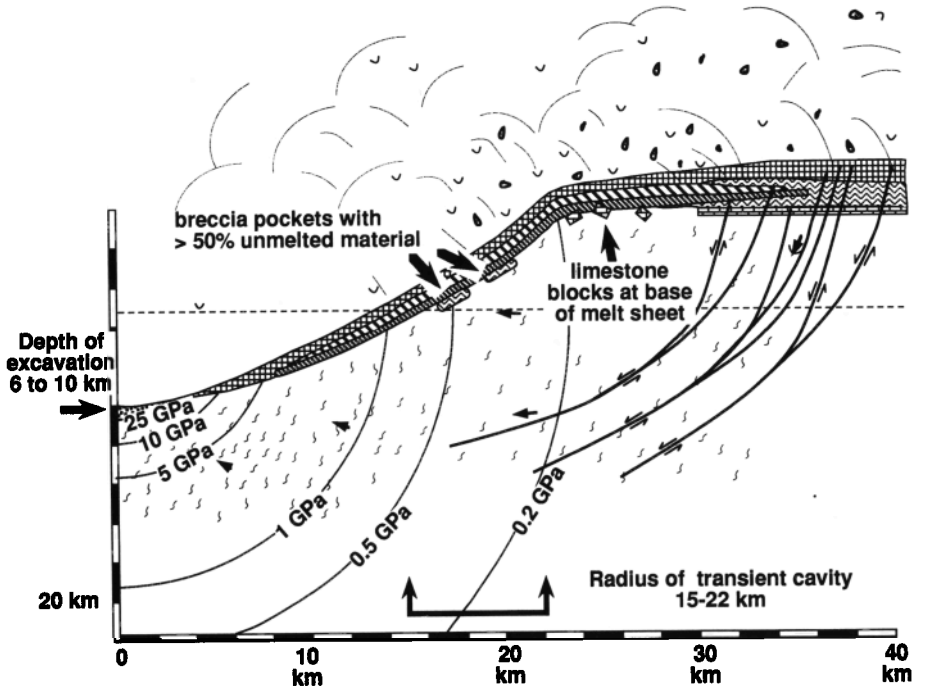


Fig. 6. Modification and terminal stages of deposition ~200 s. The time of 200 s is estimated from the time of flight for material ejected ballistically at an initial velocity of 1 km $s^{-1}$. In the transition shown here from the transient cavity to the final impact crater shape the process of central peak, or peak-ring crater formation, takes place [*Roddy*, 1968; *Shoemaker and Kieffer*, 1974]. The fine-grained clast-laden parts of the melt sheet have begun to crystallize [*Onorato et al.*, 1978] inhibiting return flow of melt to the cavity.

3 the estimated total melt sheet volume $V$ is 395 $km^3$. The remnant unshocked clasts occur only in the lower layer, for which the best estimate of thickness is 50 m, 25% of the estimated total melt sheet thickness $T_{cl}/T$. The most likely value of abundance of quartz clasts ($M_c$) is 3% of the lower layer, and the percentage abundance of quartz clasts ($M_{qc}$) is 93% of the residual clasts. $M_q$ is typically ~10%. The estimate of $V_1$ from the most likely values of the parameters is 32 $km^3$.

The best estimate that digested material constitutes 20% of the total melt sheet gives a $V_2$ value of 79 $km^3$. From this simple illustration the total amount of eroded debris incorporated into the melt sheet is $V_1 + V_2 = 111$ $km^3$. By difference (equation (2*b*)) the volume of shock melt is 284 $km^3$.

Our best estimates of the volumes $V$, $V_1$, $V_2$, and $V_{sh}$ were actually obtained from a Monte Carlo simulator in which the best estimates of each parameter were assumed to define a triangular distribution (Table 3*a*). The triangular distribution is not rigorously valid for any real distribution

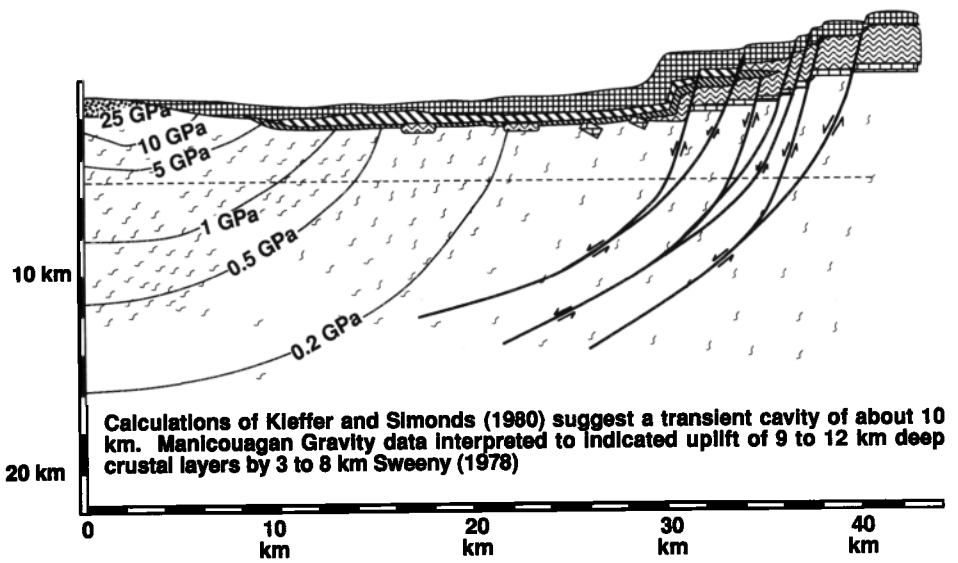


Fig. 7. Final configuration prior to erosion, Late Triassic. The fresh crater is in its final form and may look much like similar sized craters on the Moon, Mars, Venus, or even Mercury.

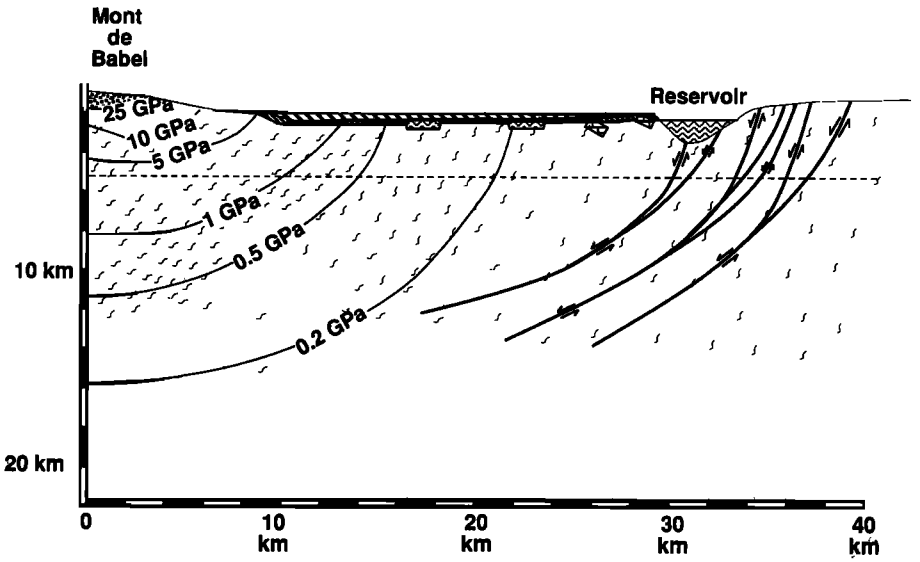


Fig. 8. Current configuration, post-Pleistocene. At Manicouagan, most of the impact-produced materials have been eroded away, including approximately half of the melt sheet. The Laurentide ice sheet eroded nearly all fragmental breccias (compare with Figure 7). The normal faults at the edge of the crater provided zones of low resistance to mechanical erosion by ice and were eroded out to form the valley now filled by the reservoir (Figure 1).

but has been used routinely in the financial community because of its ease of programming and its flexibility in accommodating estimates that are not symmetrical about a median [*Newendorp*, 1975]. In the simulator used here, 4000 trials were run with individual values for each parameter corresponding to the cumulative probability of that value equal to a computer-generated random number. The methodology was that used in financial risk analysis [*Newendorp*, 1975]. The calculations were performed using Crystal Ball®, and the results were ordered and plotted as a cumulative frequency distribution (Figure 10). The minimum estimate reflects the 16th percentile value, and the maximum corresponds to the 84th percentile, corresponding to a one standard deviation range for a normal distribution.

The estimates for the total preerosion volume $V$ of the melt sheet range from 307 to 445 km$^3$ with a median value of

TABLE 2. Manicouagan Volume Estimates

| | Ice | Permafrost | Diabase | Diabase |
|---|---|---|---|---|
| Velocity, m s$^{-1}$ | 57,700 | 57,700 | 24,600 | 17,000 |
| | | *Melt Volumes, m$^3$* | | |
| Transient cavity diameter, m | | | | |
| 60,000[a] | 5.65E+11 | 3.79E+11 | 6.52E+11 | 7.60E+11 |
| 44,000[a] | 1.73E+11 | 1.15E+11 | 1.99E+11[b] | 2.33E+11 |
| 30,000[a] | 4.07E+10 | 2.71E+10 | 4.68E+10 | 5.49E+10 |
| 60,000[c] | 3.03E+12 | 2.90E+12 | 2.11E+12 | 1.96E+12 |
| 44,000[c] | 5.76E+11 | 8.78E+11 | 9.21E+11 | 5.94E+11 |
| 30,000[c] | 2.17E+11 | 2.07E+11 | 1.52E+11 | 1.40E+11 |
| | | *Volume 25–75 GPa, m$^3$* | | |
| 60,000[d] | 6.07E+11 | 4.86E+11 | 8.17E+11 | 9.66E+11 |
| 44,000[d] | 1.83E+11 | 1.47E+11 | 2.51E+11[b] | 2.90E+11 |
| 30,000[d] | 4.30E+10 | 3.46E+10 | 5.92E+10 | 6.81E+10 |
| | | *Volume 0.2–25 GPa, m$^3$* | | |
| 60,000[d] | 3.25E+13 | 3.11E+13 | 6.59E+13 | 8.08E+13 |
| 44,000[d] | 9.82E+12 | 9.42E+12 | 2.01E+13[b] | 2.47E+13 |
| 30,000[d] | 2.31E+12 | 2.22E+12 | 4.73E+12 | 5.81E+12 |

Read 5.65E+11 as $5.65 \times 10^{11}$.

[a]Volume within 75-GPa isobar from model of *Kieffer and Simonds* [1980] iterative solution of equation (10) assuming physical properties used in that paper and assuming the projectiles sizes in Table 1.

[b]Indicates preferred estimates used to scale Figures 3–8.

[c]Melt volume estimated [*O'Keefe and Ahrens*, 1982, Figure 21] assuming $C_p$ = 7.78 km s$^{-1}$ and assuming the projectile sizes in Table 1.

[d]Assumed equal to below-ground-zero-level portion of spherical shells bounded by isobars as calculated by *Kieffer and Simonds* [1980].

TABLE 3*a*. Dimension, Material Properties, and Constants for Manicouagan Impact

| | Unit | Symbol | Minimum | Most Likely | Maximum |
|---|---|---|---|---|---|
| Petrographicaly visible clasts in clast-rich melt | % | $M_c$ | 1 | 3 | 9 |
| Quartz/total clasts still visible | % | $M_{qc}$ | 84 | 93 | 100 |
| Quartz/total target rock | % | $M_q$ | 8 | 10 | 14 |
| Thickness of lower unit | m | $T_{cr}$ | 45 | 50 | 60 |
| Thickness of upper unit | m | $T_{cp}$ | 105 | 150 | 190 |
| Total melt sheet thickness | m | $T$ | 150 | 200 | 250 |
| Inner radius, melt sheet | km | $R_{\text{inner}}$ | 7.5 | 10 | 11 |
| Outer radius, melt sheet | km | $R_{\text{outer}}$ | 22 | 27 | 30 |
| Average velocity | m s$^{-1}$ | $U$ | 100 | 750 | 1000 |
| Totally digested clast fraction (clasts shocked to >25 GPa) | % | $M_s$ | 0 | 20 | 50 |
| Depth, transient crater | km | $D_{tc}$ | 6 | 10 | 14 |
| Radius, transient crater | km | $R_{tc}$ | 15 | 22 | 30 |
| Fluid density | kg m$^{-3}$ | $\rho_f$ | 2500 | 2500 | 2500 |
| Fluid viscosity | Pa s | $\mu_v$ | 2 | 100 | 1000 |
| Boundary layer thickness | m | $\delta$ | 45 | 50 | 60 |
| Lofting coefficient | | $K$ | 0.05 | 0.05 | 0.05 |
| Karmen's constant | | $K_k$ | 0.4 | 0.4 | 0.4 |
| Flat plate constant | | $A$ | 8.0 | 8.0 | 8.0 |

378 km$^3$ (Table 3*b*). The volume of less shocked material digested ($V_1$) ranges from 18 to 50 km$^3$ with a median value of 35 km$^3$. The volume of digested more highly shocked material ($V_2$) is taken to be 0–50% of the total volume $V$ and ranges from 40 to 127 km$^3$ with a median value of 84 km$^3$. The estimates of the total volume of debris mixed into the melt sheet range from 74 to 167 km$^3$ with a median value of 121 km$^3$. The shock melt volume $V_{sh}$ ranges from 183 to 312 km$^3$ with a median value of 249 km$^3$.

The melt volume estimates obtained from field and petrographic data compare well to the amount predicted from the *Kieffer and Simonds* [1980] cratering model. In the model, all crater radii and isobars are scaled linearly with the diameter of the projectile, and all volumes are scaled as the cube of the radius. The calculations [*Kieffer and Simonds*, 1980] (Table 2), scaled to a 3450–m-diameter projectile, yield 199 km$^3$ of shock melt, a value in reasonable agreement with the 247 km$^3$ of shock melt inferred from examination of the impact melt. Other meteorite composition-velocity combinations give melt volumes between 115 and 233 km$^3$. Should the larger, 60–km-diameter transient cavity be valid, the model of *Kieffer and Simonds* [1980] yields a melt volume as high as 760 km$^3$. Still larger volumes are calculated by *O'Keefe and Ahrens* [1982] (Table 2), whose volumes range from 576 to 921 km$^3$ for a 44-km-diameter transient cavity and up to 3030 km$^3$ for a 60-km-diameter transient cavity.

### 2.5. *Erosion Rate at Manicouagan Inferred From Above Constraints*

As indicated above, the median estimated volume of impact melt (shock melt plus entrained melted and partially melted debris) is 378 km$^3$. Of this amount it is estimated that 121 km$^3$ was stripped from slower moving ejecta by the shock melt. If the average density of the stripped material was 2500 kg m$^{-3}$, the stripped mass was $3.03 \times 10^{14}$ kg. If we assume an erosion duration of 40 s (Figures 4, 5, and 10), the rate of stripping was about $7.5 \times 10^{12}$ kg s$^{-1}$.

To estimate the stripping rate per unit surface area, the surface area traversed by the flow needs to be estimated. The area stripped was assumed to consist of the transient cavity plus all surrounding area now overlain by the preserved melt sheet. The transient cavity was approximated by a half an oblate spheroid, for which the surface area $S$ is given by

$$S = \pi a^2 + \{\pi b^2 \ln [(1 + e)/(1 - e)]\}/(2e) \quad (3)$$

TABLE 3*b*. Results of Monte Carlo Simulation of Flow of Impact Melt at Manicouagan Impact

| | Unit | Symbol | 16% Minimum | 50% Medium | 84% Maximum |
|---|---|---|---|---|---|
| Volume | km$^3$ | $V$ | 307 | 378 | 445 |
| Volume eroded <25 GPa | km$^3$ | $V_1$ | 18 | 35 | 50 |
| 25–75 GPa | km$^3$ | $V_2$ | 40 | 84 | 127 |
| Total | km$^3$ | $V_1 + V_2$ | 74 | 121 | 167 |
| Volume shock melt | km$^3$ | $V_{\text{sh}}$ | 183 | 249 | 312 |
| Erosion duration | s | $t$ | 28 | 41 | 53 |
| Eroded area | km$^2$ | $S$ | 2363 | 2703 | 3030 |
| Field estimated rate | kg m$^{-2}$ s$^{-1}$ | $dm/dt$ | 1290 | 2562 | 3810 |
| Model predicted erosion rate | kg m$^{-2}$ s$^{-1}$ | $dm/dt$ | 1833 | 2598 | 3353 |

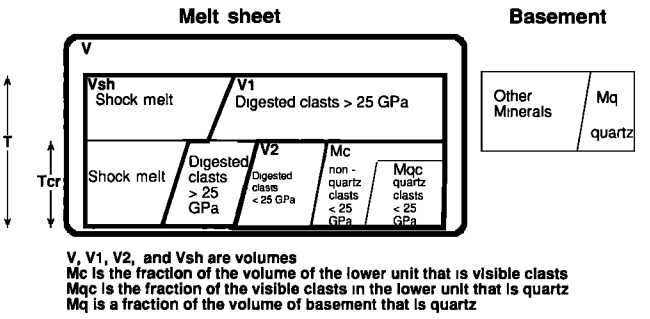


Fig. 9. Geometric relationships between parameters used to estimate the amount of material eroded at Manicouagan.

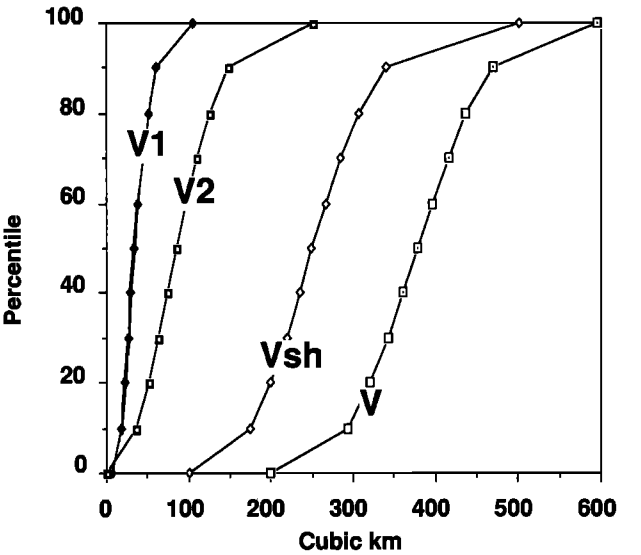


Fig. 10. Cumulative frequency plot of the results of the volume calculations for the Manicouagan impact melt sheet. The frequency scale is linear.

where $a$ and $b$ are the major and minor semiaxes, respectively, corresponding to the radius and depth of the transient cavity ($R_{tc}$ and $D_{tc}$), and $e$ is the eccentricity given by

$$e = (a^2 + b^2)^{0.5}/a = (R_{tc}^2 + D_{tc}^2)^{0.5}/R_{tc} \quad (4)$$

The area surrounding the transient cavity was approximated as a ring of outer radius $R_{\text{outer}}$ and inner radius $R_{tc}$. Thus the total area is

$$S = \pi R_{tc}^2 + \{\pi D_{tc}^2 \ln [(1 + e)/(1 - e)]\}/(2e) + \pi(R_{\text{outer}}^2 - R_{tc}^2) \quad (5)$$

Again, we illustrate these equations first by showing a calculation using the most probable values (given in Table 3*a*) before presenting the less intuitive results of the Monte Carlo calculations. For the most probable values of $R_{tc}$ = 22 km and $D_{tc}$ = 10 km the surface area of the transient cavity is calculated to be 1994 km$^2$. For the most probable values of $R_{tc}$ of 22 km and of $R_{\text{outer}}$ as 27 km the area of the ring is 770 km$^2$. The total surface area stripped using the most probable parameters is therefore 2764 km$^2$.

The Monte Carlo simulator for the stripped area gives a range from 2363 to 3030 km$^2$ with the median value being 2703 km$^2$ (Table 3*b*). Note that in this case, the assumed triangular distributions of the input parameters give a Monte Carlo median slightly less than that obtained from the most likely parameters; specifically, this is because the most likely value of $R_{tc}$ is close to the maximum value.

If the median value of total mass stripped of $3.03 \times 10^{14}$ kg was stripped from 2703 km$^2$ in 41 s, the stripping rate was 2679 kg m$^{-2}$ s$^{-1}$. The Monte Carlo technique gives a median stripping rate of 2562 kg m$^{-2}$ s$^{-1}$. Table 3*b* contains ranges for each result.

The average depth of erosion or stripping can be calculated from

$$D = (dm/dt)t/r_s \quad (6)$$

where $dm/dt$ is the stripping rate per unit area, $t$ is the event duration (40 s), and $r_s$ is the density of the stripped bedrock (2500 kg m$^{-3}$). Taking the mean value of $dm/dt$ to be equal to 2602 kg m$^{-2}$ s$^{-1}$, the average depth $D$ is 39 m.

The calculated value is not unreasonable, as field evidence supports tens of meters of stripping. Rare limestone blocks up to 10 m in dimension are included within the melt sheet in the zone 15–22 km from the center of the structure. No autochthonous limestone is observed. If the Late Triassic surface was uniformly covered by over 10 m of this limestone, then the surface outside the transient cavity was fractured and stripped down at least 10 m. The depth of erosion within the transient cavity was probably greater than outside the rim because of higher melt sheet velocities closer to the center of the crater. Also, inside the crater the flow persisted for a longer time and began at a higher velocity than it did beyond the lip of the transient cavity.

In summary, the important quantities derived from the field and petrographic work discussed above are an erosion rate of approximately 2600 kg m$^{-2}$ s$^{-1}$ and an erosion depth of several tens of meters. After introducing a summary of field observations of erosion at Mount St. Helens and reviewing a theory derived by *Kieffer and Sturtevant* [1988] for that erosion process, we apply the theory to the Manicouagan stripping problem.

## 3. Volcanic Erosion and Mixing

Evidence for erosion and mixing of substrate material into volcanic flows along their path of travel has been documented for several volcanic events. The best documented cases are two flows of very different nature at Mount St. Helens in 1980: the lateral blast on May 18 and the smaller pyroclastic flow on August 7. Erosion is evident in both cases from missing substrate material: trees, duff, and soil under the deposits of the lateral blast [*Kieffer and Sturtevant*, 1988] and missing marker nails and documented changes in channel geometry for the pyroclastic flow [*Rowley et al.*, 1981].

Mixing is well documented for the lateral blast because the basal layer is rich in organic material derived from the destruction of the forest [e.g., *Fisher*, 1990]. Mixing is less easy to demonstrate where pyroclastic flows have eroded older pyroclastic flows of similar composition and texture or volcanic rocks of similar composition. To emphasize the analogy between impact and volcanic erosion processes, we note that the admixing of the organic carbon in the lateral blast material is analogous to the mixing of moderately and weakly shocked rocks into the shock melt to form the impact

TABLE 4*a*. Dimension Estimates for the Mount St. Helens Lateral Blast

| | Unit | Symbol | Minimum | Most Likely | Maximum |
|---|---|---|---|---|---|
| Average velocity | m $s^{-1}$ | $U$ | 100 | 235 | 350 |
| Erosion duration | s | $t$ | 10 | 30 | 100 |
| Solid density | kg $m^{-3}$ | $\rho_s$ | 1000 | 1300 | 1500 |
| Fluid density | kg $m^{-3}$ | $\rho_f$ | 1 | 10 | 500 |
| Field furrow depth | m | $\Delta$ | 0.07 | 0.20 | 0.72 |
| Field general land lowering | m | $\Delta$ | 0.30 | 0.40 | 0.50 |
| Fluid viscosity | Pa s | $\mu_v$ | $2 \times 10^{-6}$ | $2 \times 10^{-5}$ | $2 \times 10^{-4}$ |
| Boundary layer thickness | m | $\delta$ | 1 | 14 | 50 |
| Lofting coefficient | | $K$ | 0.05 | 0.05 | 0.05 |
| Karmen's constant | | $K_k$ | 0.4 | 0.4 | 0.4 |
| Flat plat constant | | $A$ | 8.0 | 8.0 | 8.0 |

melt at Manicouagan. Tables 4*a* and 5*a* present estimates of the minimum, most likely, and maximum values of key parameters describing the two Mount St. Helens events.

The erosion of the land surface by the lateral blast consisted of an overall stripping of the forest and soil to tree root level and additional erosion within "furrows" at specific locations. The overall stripping is typically 0.3–0.5 m, and the furrows represent local removal of another 0.07–0.72 m [*Kieffer and Sturtevant*, 1988] (Table 2). *Kieffer and Sturtevant* [1988] attributed the erosion to a highly turbulent boundary layer and, specifically, suggested that the furrows represented geologic evidence for longitudinal vortices in the boundary layer of the blast. The duration of the blast is estimated to have ranged between 10 and 100 s with a most likely value of 30 s. Duration probably depended in a complex way on location.

The rate of erosion can be estimated from

$$dm/dt = \Delta \rho_s / t \tag{7}$$

where $dm/dt$ is the vertical rate of mass stripping (e.g., in kg $m^{-2}$ $s^{-1}$), $\Delta$ is the depth stripped, and $t$ is the duration of the event. For the furrowing part of the erosion during the lateral blast of May 18 the best estimates of each parameter are $\Delta$ = 0.2 m; $\rho_s$ = 1300 kg $m^{-3}$; and $t$ = 30 s; the furrowing erosion rate was then 9 kg $m^{-2}$ $s^{-1}$ [*Kieffer and Sturtevant*, 1988]. The total erosion rate, taking $\Delta$ = 0.4 m (overall stripping) + 0.2 m (furrowing) = 0.6 m, is then about triple that value, or 27 kg $m^{-2}$ $s^{-1}$.

We have reexamined the problem of erosion at Mount St. Helens during the lateral blast using the Monte Carlo simulator and incorporated the general lowering of the land surface as well as the furrowing (Table 4*a*). The Monte Carlo simulator gives minimum, median, and maximum values of erosion rates for the furrowing part of the erosion process as 3.5, 9.0, and 14.0 kg $m^{-2}$ $s^{-1}$ (Table 4*b*). These values are in good agreement with the estimate made by using the most probable values in the equation above. The respective Monte Carlo values for the general lowering of the land surface are 6.2, 11.5, and 16.3 kg $m^{-2}$ $s^{-1}$, approximately the same magnitude as the furrowing rates. The best estimate of the total erosion rate estimated from field evidence is 20.6 kg $m^{-2}$ $s^{-1}$ with a range from 10.3 to 30.0 kg $m^{-2}$ $s^{-1}$ from the Monte Carlo simulator.

A relatively small pyroclastic flow on August 7, 1980, eroded grooves and channels into pre-1980 volcanic rocks consisting of well-consolidated breccias, lava flows, and tuff [*Rowley et al.*, 1981]. Nails of 16-cm length driven into the walls of the preexisting channel in the Stairsteps were removed by the flow, and the channel showed erosion to depths of "several meters." We assume that the erosion removed 0.5–3 m of dense rock with a best estimate of 2 m. The erosion occurred where measured and calculated velocities in the channel were highest [*Rowley et al.*, 1981] based on analysis of movies by *Hoblitt* [1986] and theory by *Levine and Kieffer* [1991]. The duration of the flow as documented in the movies of the event was 390 s. Here we estimate possible values of the erosive phase to range from 200 to 390 s with a most likely value of 300 s.

To estimate an erosion rate during the pyroclastic flow of August 7, 1980, we assume the most likely value of 2 m of erosion. We assume that the pyroclastic flow lasted for 5 min [*Levine and Kieffer*, 1991] and that the substrate density was 2400 kg $m^{-3}$. The erosion rate, then, would be 16 kg $m^{-2}$ $s^{-1}$ (Table 5*b*). The Monte Carlo simulator gives a range of

TABLE 4*b*. Results of Monte Carlo Simulations for the Mount St. Helens Lateral Blast

| | Unit | Symbol | 16% Minimum | 50% Medium | 84% Maximum |
|---|---|---|---|---|---|
| Field predicted furrow erosion rate | kg $m^{-2}$ $s^{-1}$ | $dm/dt$ | 3.5 | 9.0 | 14.0 |
| Field predicted general land lowering rate | kg $m^{-2}$ $s^{-1}$ | $dm/dt$ | 6.2 | 11.5 | 16.3 |
| Field predicted total erosion rate | kg $m^{-2}$ $s^{-1}$ | $dm/dt$ | 10.3 | 20.6 | 30.0 |
| Model predicted erosion rate | kg $m^{-2}$ $s^{-1}$ | $dm/dt$ | 6.0 | 29.5 | 53.0 |
| Model predicted erosion depth | m | $\Delta$ | 0.12 | 0.97 | 1.77 |

9.3–19.1 kg $m^{-2}$ $s^{-1}$ with a median estimate of 14.3 kg $m^{-2}$ $s^{-1}$.

In section 4 we present a theoretical method for estimating erosion rates and compare the results with the rates estimated from field data for Manicouagan (2600 kg $m^{-2}$ $s^{-1}$), the Mount St. Helens lateral blast (total rate 21 kg $m^{-2}$ $s^{-1}$), and the August 7, 1980, pyroclastic flow (14 kg $m^{-2}$ $s^{-1}$).

## 4. Theoretical Estimate of Erosion Rate

The theory is an empirical model for the rate of erosion under a turbulent boundary layer in high-speed flow [*Kieffer and Sturtevant*, 1988]. All the flows are turbulent with the exception of the Mount St. Helens pyroclastic flow under the extreme case that the density was at the high end of the plausible range. Reynolds numbers for the flows (see Tables 2*a*, 3*b*, 4*a*, and 5*a* for parameters) range from $7.5 \times 10^2$ to $7.5 \times 10^5$ for the Mount St. Helens pyroclastic flow, $2.8 \times 10^5$ for Manicouagan, and $1.9 \times 10^{10}$ for the Mount St. Helens lateral blast. Laboratory [*Hartenbaum*, 1971] and field [*Kieffer and Sturtevant*, 1988] experiments suggest that the time-averaged vertical mass flux per unit surface area, the stripping rate, is proportional to the density $\rho_f$ and the friction velocity $u_t$:

$$dm/dt = K\rho_f u_t \tag{8}$$

where $K$ is an empirically determined constant called the "lofting efficiency." The friction velocity is proportional to the square root of the shear stress $\tau$ exerted by the flow on the ground:

$$u_t = (\tau/\rho_f)^{1/2} \tag{9}$$

The friction velocity is obtained from turbulent boundary layer theory as

$$U/u_t = (1/\kappa_k) \ln (\rho_f u_\tau \delta/\mu_v) + A \tag{10}$$

where $U$ is the free-stream velocity, $\kappa_k = 0.4$ is Karman's constant for the logarithmic friction law, $\mu_v$ is the Newtonian viscosity, $\delta$ is the boundary layer thickness, and $A$ is a constant, taken as $A \sim 8$ for flat plates. The depth of erosion ($\Delta$) is then

$$\Delta = KUt(\rho_f/\rho_s)(u_\tau/U) \tag{11}$$

The equation is written in this particular form to emphasize that to first order the erosion rate (or depth eroded) depends nearly linearly on $U$ and $\rho_f$, as shown by combining equations (10) and (11), so we refer to this loosely as "momentum scaling." However, second-order effects arise in the friction velocity (equation (10)), and in our calculations we have solved the relevant equations exactly using an iterative technique.

The lofting model equates the vertical momentum of the particulates lofted from a bed to a fraction of the horizontal impulse delivered to the particle layer per unit time by the abrading substance. The vertical velocity of the particles is set equal to some fraction of the shear stress velocity. The lofting efficiency $K$ accounts for these two fractions and is herein taken as 0.05 (*Hartenbaum* [1971]; see also *Kieffer and Sturtevant* [1988] for further discussion of the theory and choice of numerical values used below).

Each parameter in the equations has restrictions and uncertainties associated with it, not all of which can be discussed in detail here. For the calculations, Karman's constant $\kappa_k$ is taken to be the same for all cases (0.4), as is the "flat plate constant" $A(\sim 8)$. Values of the parameters $U$, $t$, $\rho_s$, $\rho_f$, $\Delta$, and $\delta$ can be found in references cited in section 5. The mean fluid viscosity $\mu_v$ was taken as that of steam at 650°K for the Mount St. Helens lateral blast and as that of steam at 1100°K for the low-density pyroclastic flow and was estimated from the field for a high-density pyroclastic flow [*Wilson and Head*, 1981].

*Kieffer and Sturtevant* [1988] solved the above equations using the mean values of the parameters given in Table 4*a* and found that the theory gave an erosion rate of 2.5 kg $m^{-2}$ $s^{-1}$, approximately a factor of 4 less than the rate inferred from the depth of the furrows, and concluded that the lofting coefficient $K$ might therefore be at least a factor of 4 enhanced by the furrowing process (longitudinal vortices in the boundary layer). The enhancement would be even larger if the general lowering of the land surface was accounted for in their model. In the following discussion we include the general lowering of the land surface as well as the furrows in our discussion of erosion. Therefore this treatment is different from the earlier treatment in two respects: we are looking at the overall erosion rate instead of just the furrowing erosion, and we use Monte Carlo techniques instead of average values to obtain estimates. These two differences account for an apparent difference in results, but the results from the two studies are compatible except as noted.

The Monte Carlo simulations for the Mount St. Helens lateral blast give substantially different results than the Kieffer-Sturtevant results because of the skewed distributions in minimum, most likely, and maximum probable values of the parameters. The median predicted value for the total erosion during the Mount St. Helens lateral blast (general surface lowering plus furrowing) is 29.5 kg $m^{-2}$ $s^{-1}$ with a range from 6.0 to 53.0 kg $m^{-2}$ $s^{-1}$ compared with the field estimate of 20.6 kg $m^{-2}$ $s^{-1}$, with a range from 10.3 to 30.0 kg $m^{-2}$ $s^{-1}$ (Table 4*b*). We consider this agreement to be excellent.

Because the agreement between field and theory is so good when Monte Carlo techniques are used to include estimates of uncertainty we conclude that the theory works without enhancement of the erosional efficiency by the furrowing process, although this argument does not rigorously preclude an enhanced efficiency $K$. It is worth keeping in mind that the efficiency, as represented in the lofting coefficient, is simply a "fudge factor" relating to transfer of momentum [*Hartenbaum*, 1971], and that there is no a priori reason to believe that it should have the same value in different field situations as in the laboratory experiments. The relatively good agreement between calculated and field-constrained lofting equations for two erosion events different in origin and scale (meteonte impact and volcanic) suggests that erosion during large-scale, high-velocity events might be estimated by relatively simple lofting theory.

We had the good fortune to obtain partial data during another erosion situation while this paper was under revision and have included this paragraph with permission of the editor. On January 8, 1993, the Salt River, Arizona, rose into dramatic flood stage, causing erosion of the Tri-City Landfill. During 1 hour of the rising stage of the flood the landfill bank was measured to recede at a rate of 9 m/h (P. Likens, personal communication, 1993). Assuming a landfill density of 1500 kg/$m^3$ (range 1400–1600 kg/$m^3$) and a duration of 1

TABLE 5a. Dimension Estimates for the Mount St. Helens Pyroclastic Flow With High Densities

| | Unit | Symbol | Minimum | Most Likely | Maximum |
|---|---|---|---|---|---|
| Average velocity | m $s^{-1}$ | $U$ | 20 | 25 | 30 |
| Erosion duration | s | $t$ | 200 | 300 | 390 |
| Solid density | kg $m^{-3}$ | $\rho_s$ | 1900 | 2400 | 2700 |
| Fluid density | kg $m^{-3}$ | $\rho_f$ | 1000 | 1200 | 1500 |
| Fluid viscosity | Pa s | $\mu_v$ | 2 | 4 | 8 |
| Field overall erosion depth | m | $\Delta$ | 0.5 | 2 | 3 |
| Boundary layer thickness | m | $\delta$ | 1 | 2 | 3 |
| Lofting coefficient | | $K$ | 0.05 | 0.05 | 0.05 |
| Karmen's constant | | $K_k$ | 0.4 | 0.4 | 0.4 |
| Flat plate constant | | $A$ | 8.0 | 8.0 | 8.0 |

hour, the measured erosion rate was 3.8 kg $m^{-2}$ $s^{-1}$. We justified using the lofting theory for bed scour to this bank scour situation by noting that the mechanism of transport of the bank material was undercutting and slumping of the bank into the river and then lofting of the slumped material into the flow. The erosion theory predicts a rate of 9.6 kg $m^{-2}$ $s^{-1}$. This overestimate of the rate by the theory may reflect a decrease in efficiency for this bank scour situation.

Finally, to use this theory in yet another situation, we applied the above equations to the August 7, 1980, pyroclastic flow documented by *Wilson and Head* [1981] to investigate the controversy regarding inflated (surgelike) and deflated (flowlike) character [*Fisher*, 1983, 1990; *Valentine*, 1987]. If we use the standard assumptions of pyroclastic flow theory [*Walker and McBroome*, 1984] that the flow has approximately the same density and viscosity during movement as it does in the deposit, the erosion rates predicted by the model are a factor of 4.5 too high (see Tables 5a and 5b). Because there is no overlap (1 standard deviation) between the model and field ranges, the high-density hypothesis may be rejected on statistical grounds [*Bhattacharya and Johnson*, 1977, chapter 6]. If we adopt a set of assumptions more consistent with surgelike inflated characteristics, the erosion rates from the model are within 50% of the field-estimated values (see Tables 6a and 6b). Because there is overlap of the model and field ranges, the low-density hypothesis is statistically acceptable. The choice of fluid density and 250 kg $m^{-3}$ is, however, obviously arbitrary and picked to optimize the model.

We speculate that the August 7, 1980, pyroclastic flow was changing from surgelike to flowlike characteristics as it traversed different parts of the channel. We suspect that it may have been inflated and surgelike in the Stairsteps where the nails were eroded. This theory is consistent with the results of *Levine and Kieffer* [1991], in which they found that depths calculated under the assumption of incompressible flow were too shallow in the Stairsteps to account for the erosion of the nails. Nails were eroded as high as 10 m up on the walls. Calculated flow depths for a flow with the density of the final deposit in the same reaches were only 6–9 m. Because the calculated depths do not account for additional lowering of the channel bottom by erosion, the discrepancy between the hydraulic model and the field evidence is even greater than these numbers indicate, so we conclude that the flow could have been inflated by several meters equivalent depth. None of these pieces of evidence alone can completely resolve the existing controversies of the nature of flows and surges, but the combined evidence suggests that at least part of the flow operates in the inflated (surgelike) regime.

## 5. Discussion

### 5.1. *Comparison of the Mixing Processes Due to Impact and Volcanic Eruptions*

There has been little theoretical work done on the mixing processes that occur during large impact or volcanic eruptions, and much experimental work that has been done is at an inappropriately small scale (e.g., particulate abrasion by dilute gases, small-scale scour in river channels). However, the observations of mixed lithics, organics, and tephra that abound in the volcanic literature about pyroclastic flows and blasts and the geochemical and petrologic data presented here about the Manicouagan melt sheet demonstrate that this process is important in the evolution of the ejecta along their travel paths.

Mixing in volcanically induced flows may be the conceptually simpler process to understand. Erosion occurs primarily along a basal shear zone along a well-defined ground surface, although secondarily, erosion may occur in an enlarging conduit or crater near the vent. Along the ground surface the velocity gradients are steep, and shear and mixing occur through this zone.

TABLE 5b. Monte Carlo Simulations for the Mount St. Helens Pyroclastic Flow With High Densities

| | Unit | Symbol | 16% Minimum | 50% Medium | 84% Maximum |
|---|---|---|---|---|---|
| Field erosion rate | kg $m^{-2}$ $s^{-1}$ | $dm/dt$ | 9.3 | 14.3 | 19.1 |
| Model predicted erosion rate | kg $m^{-2}$ $s^{-1}$ | $dm/dt$ | 56.7 | 64.3 | 71.7 |
| Predicted erosion depth | m | $\Delta$ | 6.6 | 8.2 | 9.8 |

TABLE 6*a*. Fluid Property Estimates for the Mount St. Helens Pyroclastic Flow With Low Densities

| | Unit | Symbol | Minimum | Most Likely | Maximum |
|---|---|---|---|---|---|
| Fluid density | kg $m^{-3}$ | $\rho_f$ | 1 | 250 | 500 |
| Fluid viscosity | Pa s | $\mu_\nu$ | 4 $10^{-6}$ | 4 $10^{-5}$ | 4 $10^{-4}$ |

Mixing in impact-induced flows is much more complicated because of the nature of the waxing and waning development of the transient cavity and the flow field outside of the cavity. We speculate on this process as follows: First, mixing will occur only in regions where substantial shear develops, and second, recognizable mixing will occur only where the shear zones cross original bedrock lithologic boundaries or isobars of constant degree of shock. Shear is inevitable in the subspherical geometry and radial flow typical of impact craters, and it is enhanced by the steep velocity decay outward from the center of impact. For example, numerical calculations of flow fields during impact [*O'Keefe and Ahrens*, 1975, 1976; *Orphal*, 1977*a*, *b*] suggest that at ~3 s into an impact the maximum flow velocities are over 1000 m $s^{-1}$ at depths of 12 km and less than 250 m $s^{-1}$ at further depths of over 25 km. By 50 s the faster material has slowed down to less than 250 m $s^{-1}$. The flow field has a spherically symmetric expansion of materials subradially from the center of impact established by the compressional shock. Gravity and inertial effects restrain the motion of the free surface. As the compressional phase decays, the spherical geometry disappears because the velocity vectors rotate to become subparallel to the free surface and then begin to displace the free surface itself. Thus, in Manicouagan-sized impacts the surfaces over which large shears occur migrate throughout much of the excavated volume, resulting in mixing of constituents initially separated by many kilometers. It has been suggested (E. M. Shoemaker, private communication, 1992) that shear heating during flow accounts for some of the melting and homogenization of the melt sheet.

Although the theoretical calculations presented here overly simplify a very complex geologic process, their value may be in demonstrating that the seemingly smaller erosive power of the volcanic events (as expressed in the mass stripping rate) is not a consequence of their lower speeds or their shorter duration. In fact, the velocities of the flows (several hundreds of meters per second) are comparable in both cases, as are the durations. The greater eroding power of the impact-induced flows is largely a consequence of the higher density of the eroding fluid. If the ejecta produced by an impact event had a lower density than melt, we would expect the erosive power to be correspondingly reduced if all other variables were the same. This hypothesis could perhaps be tested in models of suevite formation.

### 5.2. *Implications for Remote and Sample Observations of Asteroids, Natural Satellites, and Planets*

*Mixing and resetting of ages.* A spectacular effect of impact is intense mixing down to scales less than a millimeter. The bulk geochemical data at Manicouagan suggest that individual 1.5 × $10^{-3}$ kg samples include material from several different major parts of the metamorphosed layered igneous complex of the target. The complex ranges from anorthositic to gabbroic and mafic in composition and has a substantial fraction of the quartzo-feldspathic gneisses. The geochemical data are interpreted to suggest that target rocks are mixed by a process so intense that it can combine materials on a fine scale in a flow time measured in tens of seconds. Interestingly enough, although the target rocks are intensely mixed, the melt does not appear to be exposed to the melted or vaporized projectile. One explanation of this is that the projectile was ice. However, a different, dynamic interpretation of this is that a melt sheet includes little material that was vaporized close to the projectile. The meteorite-contaminated material may have gone into a cloud of vaporized target, similar to processes suggested by *Vickery and Melosh* [1990], and ultimately into the clays formed by hydrolysis of the fine silicate dust or possibly tektites.

*Bias in mineralogy.* The mineralogy of impact melt rocks does not necessarily correspond to a simple paragenetic sequence for a crystallizing melt of a given bulk composition because of the mixing process. In the impact melt rock at Manicouagan the relict clasts are dominantly quartz, while the liquidus phase is plagioclase feldspar. In the lunar samples the liquidus phase is a calcic plagioclase, while the relict clasts are plagioclase even more calcic than the liquidus compositions, $An_{96+}$.

*Mixing and early crustal evolution.* *Grieve et al.* [1991] demonstrate that the composition and isotopic systematics of the 2.5-km-thick melt sheet at the Sudbury, Quebec, structure are consistent with its origin as a bulk melt of the crust of the Canadian Shield at the time of impact. They argue that the well-documented crystal-settling fractionation

TABLE 6*b*. Monte Carlo Simulations for the Mount St. Helens Pyroclastic Flow With Low Densities

| | Unit | Symbol | 16% Minimum | 50% Medium | 84% Maximum |
|---|---|---|---|---|---|
| Field erosion rate | kg $m^{-2}$ $s^{-1}$ | $dm/dt$ | 9.3 | 14.3 | 19.1 |
| Model predicted erosion rate | kg $m^{-2}$ $s^{-1}$ | $dm/dt$ | 4.2 | 7.4 | 10.5 |
| Model predicted erosion depth | m | $\Delta$ | 0.5 | 0.9 | 1.4 |

of the Sudbury melt sheet is a consequence of the great thickness and slow cooling. Sudbury contains a clast-rich zone at the base of the igneous complex, as does Manicouagan. It seems plausible that the type of intense mixing of crustal material, demonstrated at Manicouagan and modeled theoretically in this paper, is characteristic of large impacts. The mixing of the superheated shock melt with a nearly equal mass of other debris to form a laterally and vertically homogeneous body of melt is possibly characteristic of the early planetary bombardment prior to about 3.9 Ga. The thickest of these bodies of melt, then, may be able to fractionate by crystal settling to yield the range of both cumulate and crystal residual compositions that make up the highland crust of the Moon. As at Manicouagan, these igneous bodies would preserve little of the chemical signature of the impacting body. They would generally be inferred to be the products of endogenic igneous processes. However, the bodies would be the fractionated derivatives of mixtures of crustal compositions, as is true at Sudbury.

*Acknowledgments.* Charles H. Simonds' work was supported by Lockheed Missiles and Space Company Inc., funds. Susan W. Kieffer was supported by NASA.

## REFERENCES


Ahrens, T. J., and J. D. O'Keefe, Equations of state and impact induced shock wave attenuation on the moon, in *Impact and Explosion Cratering*, edited by D. J. Roddy, R. O. Pepin, and R. B. Merrill, pp. 939–956, Pergamon, New York, 1977.

Ahrens, T. J., and J. D. O'Keefe, Impact on the Earth ocean and atmosphere, *Int. J. Impact Eng.*, *5*, 13–32, 1987.

Bhattacharya, G. K., and R. A. Johnson, *Statistical Concepts and Methods*, 639 pp., John Wiley, New York, 1977.

Dence, M. R., The extraterrestrial origin of Canadian craters, *Ann. N. Y. Acad. Sci.*, *123*, 941–969, 1965.

Dence, M. R., R. A. F. Grieve, and P. B. Robertson, Terrestrial impact structures: Principal characteristics and energy considerations, in *Impact and Explosion Cratering*, edited by D. J. Roddy, R. O. Pepin, and R. B. Merrill, pp. 247–275, Pergamon, New York, 1977.

Dressler, B., Die Beanspruchung der Prakambrischen Gesteine in der Kryptoexplosionsstruktur von Manicouagan in der Provinz Quebec, Canada, doctoral dissertation, 99 pp., Ludwig-Maximilians Univ., Munich, 1970.

Fisher, R. V., Flow transformations in sediment gravity flows, *Geology*, *11*, 273–274, 1983.

Fisher, R. V., Transport and deposition of a pyroclastic surge across an area of high relief: On 18 May 1980 eruption of Mount St. Helens, *Geol. Soc. Am. Bull.*, *102*, 1038–1054, 1990.

Floran, R. J., R. A. F. Grieve, W. C. Phinney, J. L. Warner, C. H. Simonds, D. P. Blanchard, and M. R. Dence, Manicouagan impact melt Quebec, 1, Stratigraphy, petrology, and chemistry, *J. Geophys. Res.*, *83*, 2737–2760, 1978.

French, B. M., and N. M. Short, *Shock Metamorphism of Natural Materials*, 644 pp., Mono, Baltimore, Md., 1968.

Grieve, R. A. F., and R. J. Floran, Manicouagan impact melt Quebec, 2, Chemical interrelations with basement and formational processes, *J. Geophys. Res.*, *83*, 2761–2771, 1978.

Grieve, R. A. F., and J. W. Head, Manicouagan impact structure: An analysis of its original dimensions and form, *Proc. Lunar Planet. Sci. Conf. 13th*, Part 2, *J. Geophys. Res.*, *88*, suppl., A807–A818, 1983.

Grieve, R. A. F., D. Stoffler, and A. Deutsch, The Sudbury structure: Controversial or misunderstood?, *J. Geophys. Res.*, *96*, 22,753–22,764, 1991.

Hartenbaum, B., Lofting of particulates by a high speed wind, *Rep. DNA-2737*, 73 pp., Def. Nucl. Agency, Washington, D. C., 1971.

Hoblitt, R. P., Observations of eruptions of July 22 and August 7, 1980 at Mount St. Helens, Washington, *U.S. Geol. Surv. Prof. Pap.*, *1355*, 44 pp., 1986.

Holsapple, K. A., and R. M. Schmidt, Point source solutions and coupling parameters in cratering mechanics, *J. Geophys. Res.*, *92*, 6350–6376, 1987.

Jahn, B. M., R. J. Floran, and C. H. Simonds, Rb-Sr isochron age of Manicouagan melt sheet, *J. Geophys. Res.*, *83*, 2799–2804, 1978.

Kieffer, S. W., Fluid dynamics of the May 18 blast at Mount St. Helens, *U.S. Geol. Surv. Prof. Pap.*, *1250*, 379–400, 1981.

Kieffer, S. W., Factors governing the structure of volcanic jets, in *Explosive Volcanism: Inception, Evolution, and Hazards*, vol. 11, edited by F. M. Boyd, pp. 143–157, National Academy of Sciences, Washington, D. C., 1984.

Kieffer, S. W., and C. H. Simonds, The role of volatiles and lithology in the impact cratering process, *Rev. Geophys.*, *18*, 143–181, 1980.

Kieffer, S. W., and B. Sturtevant, Erosional furrows formed during the lateral blast at Mount St. Helens, May 18, 1980, *J. Geophys. Res.*, *93*, 14,793–14,816, 1988.

Levine, A. H., and S. W. Kieffer, Hydraulics of the August 7, 1980 pyroclastic flow at Mount St. Helens, Washington, *Geology*, *19*, 1121–1124, 1991.

Lipman, P. W., and D. R. Mullineaux (Eds.), The 1980 eruptions at Mt. St. Helens, Washington, *U.S. Geol. Surv. Prof. Pap.*, *1250*, 884 pp., 1981.

McQueen, R. G., S. P. Marsh, and J. N. Fritz, Hugoniot equations of state of twelve rocks, *J. Geophys. Res.*, *72*, 4999–5036, 1967.

Melosh, H. J., *Impact Cratering: A Geologic Process*, 245 pp., Oxford University Press, New York, 1989.

Newendorp, P. D., *Decision Analysis for Petroleum Exploration*, 668 pp., PennWell, Tulsa, Okla., 1975.

O'Keefe, J. D., and T. J. Ahrens, Shock effects of a large impact on the Moon, *Proc. Lunar Sci. Conf.*, *6th*, 2831–2844, 1975.

O'Keefe, J. D., and T. J. Ahrens, Impact ejecta on the Moon, *Proc. Lunar Sci. Conf.*, *7th*, 3007–3026, 1976.

O'Keefe, J. D., and T. J. Ahrens, Cometary and meteorite swarm impact on planetary surfaces, *J. Geophys. Res.*, *87*, 6668–6680, 1982.

Olsen, P. E., and P.-E. Sues, Correlation of continental Late Triassic and Early Jurassic sediments, and patterns of the Triassic-Jurassic tetrapod transition, in *The Beginning of the Age of Dinosaurs, Faunal Change Across the Triassic-Jurassic Boundary*, edited by K. Padian, pp. 321–351, Cambridge University Press, New York, 1984.

Onorato, P. I. K., D. R. Uhlmann, and C. H. Simonds, Thermal history of Manicouagan melt sheet, *J. Geophys. Res.*, *83*, 2789–2798, 1978.

Orphal, D., Calculation of explosion cratering, I, The shallow-buried nuclear detonation JOHNIE BOY, in *Impact and Explosion Cratering*, edited by D. J. Roddy, R. O. Pepin, and R. B. Merrill, pp. 897–906, Pergamon, New York, 1977*a*.

Orphal, D., Calculation of explosion cratering, II, Cratering mechanics and phenomenalogy, in *Impact and Explosion Cratering*, edited by D. J. Roddy, R. O. Pepin, and R. B. Merrill, pp. 907–917, Pergamon, New York, 1977*b*.

Palme, H., Indentification of projectiles of large terrestrial impact craters and some implications for the interpretation of Ir-rich Cretaceous/Tertiary boundary layers, in Geological Implications of Impacts of Large Asteroids and Comets on the Earth, edited by L. T. Silver and P. H. Schultz, *Spec. Pap., Geol. Soc. Am.*, *190*, 223–233, 1982.

Phinney, W. C., M. R. Dence, and R. A. F. Grieve, Investigation of the Manicouagan impact crater, Quebec: An introduction, *J. Geophys. Res.*, *83*, 2729–2735, 1978.

Roddy, D. J., The Flynn Creek crater, in *Shock Metamorphism of Natural Materials*, edited by B. M. French and N. M. Short, pp. 291–322, Mono, Baltimore, Md., 1968.

Rowley, P. D., M. A. Kuntz, and N. S. MacLeod, Pyroclastic flow deposits, *U.S. Geol. Surv. Prof. Pap.*, *1250*, 489–512, 1981.

Schmidt, R. M., and K. A. Holsapple, Estimates of crater size for large body impact: Gravity scaling results, in Geological Implications of Impacts of Large Asteroids and Comets on the Earth, edited by L. T. Silver and P. H. Schultz, *Spec. Pap. Geol. Soc. Am.*, *190*, 93–102, 1982.

Schmidt, R. M., and K. R. Housen, Some recent advances in the scaling of impact and explosion cratering, *Int. J. Impact Eng.*, *5*, 543–560, 1987.

Shoemaker, E. M., Impacts of the Meteor Crater, Arizona, in *Moon, Meteorites, and Comets*, edited by B. M. Middlehurst and G. P. Kuiper, pp. 301–336, University of Chicago Press, Chicago, Ill., 1963.

Shoemaker, E. M., Astronomically observable crater-forming projectiles, in *Impact and Explosion Cratering*, edited by D. J. Roddy, R. O. Pepin, and R. B. Merrill, pp. 617–628, Pergamon, New York, 1977.

Shoemaker, E. M., and S. W. Kieffer, Guidebook to the geology of Meteor Craters, *Publ. 17*, Inst. of Meteorit. Stud., Tempe, Ariz., 1974.

Shoemaker, E. M., R. M. Wolfe, and C. S. Shoemaker, Asteroid and comet flux in the neighborhood of Earth, in Global Catastrophies in Earth History: An Interdisciplinary Conference on Impacts Volcanism and Mass Mortality, edited by V. L. Sharpton and P. D. Ward, *Spec. Pap. Geol. Soc. Am.*, *247*, 155–170, 1990.

Simonds, C. H., R. J. Floran, P. E. McGee, W. C. Phinney, and J. L. Warner, Petrogenesis of melt rocks, Manicouagan impact structure, Quebec, *J. Geophys. Res.*, *83*, 2773–2788, 1978.

Sweeny, J. F., Gravity study of a great impact, *J. Geophys. Res.*, *83*, 2809–2816, 1978.

Valentine, G. A., Stratified flow in pyroclastic surges, *Bull. Volcanol.*, *49*, 616–630, 1987.

Valentine, G. A., and K. H. Wohletz, Numerical models of Plinean eruption columns and pyroclastic flows, *J. Geophys. Res.*, *94*, 1867–1887, 1989.

Valentine, G. A., and K. H. Wohletz, Sources of unsteady column dynamics in pyroclastic flow eruptions, *J. Geophys. Res.*, *96*, 21,887–21,892, 1991.

Valentine, G. A., K. H. Wohletz, and S. W. Kieffer, Effects of topography on facies and compositional zonation in caldera-related ignimbrites, *Geol. Soc. Am. Bull.*, *104*, 154–165, 1992.

Vickery, A. M., and H. J. Melosh, Atmospheric erosion and impactor retention in large impacts, with application to mass extinctions, in Global Catastrophies in Earth History: An Interdisciplinary Conference on Impacts Volcanism and Mass Mortality, edited by V. L. Sharpton and P. D. Ward, *Spec. Pap. Geol. Soc. Am.*, *247*, 289–300, 1990.

Walker, G. P. L., and L. A. McBroome, Comments and reply on "Mount St. Helens 1980 and Mount Pelee 1902—Flow or surge?", *Geology*, *12*, 693–695, 1984.

Wilson, L., and J. W. Head, Morphology and rheology of pyroclastic flows and their deposits and guidelines for future observations, *U.S. Geol. Surv. Prof. Pap.*, *1250*, 513–524, 1981.

Wilson, L., H. Pinkerton, and R. MacDonald, Physical processes of volcanic eruptions, *Annu. Rev. Earth Planet. Sci.*, *15*, 73–95, 1987.

Wohletz, K. H., T. R. McGetchin, M. T. Sanford II, and E. M. Jones, Hydrodynamic aspects of caldera-forming eruptions, *J. Geophys. Res.*, *89*, 8269–8286, 1984.

Wolfe, S. H., Potassium-argon ages of the Manicouagan-Mushalagan lakes structure, *J. Geophys. Res.*, *76*, 5424–5436, 1971.

Zook, H. A., The state of meteoritic material on the moon, *Proc. Lunar Sci. Conf.*, *6th*, 1653–1672, 1975.

S. W. Kieffer, Department of Geology, Arizona State University, Tempe, AZ 85287-1404.

C. H. Simonds, Space Station EVA Systems, Lockheed Missiles & Space Co., Inc., Mail Code A-23, 1150 Gemini Avenue, Houston, TX 77058-2742.

(Received June 5, 1992;
revised March 1, 1993;
accepted March 10, 1993.)